

Testing the Nambu-Goldstone Hypothesis for Quarks and Leptons at the LHC

Sourav K. Mandal^{1,2}, Mihoko Nojiri^{2,3,4}, Matthew Sudano^{2,5} and Tsutomu T. Yanagida^{2,6}

¹*Department of Physics, University of California
Berkeley, CA 94720, USA*

²*Institute for the Physics and Mathematics of the Universe, University of Tokyo
Kashiwa, Chiba 277-8583, Japan*

³*Theory Group, KEK, Tsukuba, Ibaraki 305-0801, Japan*

⁴*The Graduate University for Advanced Studies (SOKENDAI)
Tsukuba, Ibaraki 305-0801, Japan*

⁵*School of Natural Sciences, Institute for Advanced Study
Princeton, NJ 08540, USA*

⁶*Department of Physics, Graduate School of Science, University of Tokyo
Tokyo 113-0033, Japan*

Abstract

The hierarchy of the Yukawa couplings is an outstanding problem of the standard model. We present a class of models in which the first and second generation fermions are SUSY partners of pseudo-Nambu-Goldstone bosons that parameterize a non-compact Kähler manifold, explaining the small values of these fermion masses relative to those of the third generation. We also provide an example of such a model. We find that various regions of the parameter space in this scenario can give the correct dark matter abundance, and that nearly all of these regions evade other phenomenological constraints. We show that for $m_{\tilde{g}} \sim 700$ GeV, model points from these regions can be easily distinguished from other mSUGRA points at the LHC with only 7 fb^{-1} of integrated luminosity at 14 TeV. The most striking signatures are a dearth of b - and τ -jets, a great number of multi-lepton events, and either an “inverted” slepton mass hierarchy, narrowed slepton mass hierarchy, or characteristic small- μ spectrum.

1 Introduction

One of the fundamental problems in particle physics is to explain the hierarchy in the Yukawa couplings of the quarks and leptons. This is a long-standing problem, and in fact many models have been proposed to account for the smallness of the Yukawa couplings of the first and second generations relative to those of the third. In supersymmetric (SUSY) theories, there arises an intriguing possibility that the quarks and leptons are nothing but SUSY partners of Nambu-Goldstone (NG) bosons [1, 2], where the Yukawa couplings are forbidden by the celebrated low-energy theorem [3]. Thus, the small Yukawa couplings for the first and second generations are regarded as small breakings of postulated symmetries.

If that is indeed the case, then squarks and sleptons in the first and second generations are approximately massless at some cut-off scale Λ of the theory and they acquire masses from radiative corrections. If the corrections are dominated by the standard model gauge interactions, then they each have nearly flavor-independent masses, solving the SUSY flavor-changing neutral current problem. This hypothesis predicts a remarkable spectrum for SUSY particles at the electroweak scale. The purpose of this paper is to examine the low-energy implications of the Nambu-Goldstone hypothesis.

It is very important to note here that if the Kähler manifold parameterized by the NG bosons is a compact manifold such as \mathbf{CP}^n , the symmetry is explicitly broken by a constant term $\mathcal{O}(m_{3/2})$ in the superpotential [4]¹. As a consequence of the explicit breaking, the NG bosons have masses of $\mathcal{O}(m_{3/2})$, and it will be not easy to test the NG hypothesis at the LHC. Thus, we consider in this paper some non-compact complex manifold (non-linear sigma model) accommodating squarks and sleptons in the first and second generations as massless NG bosons. (The results in this paper do not depend on the explicit model for the non-compact complex manifold. We show it for the existence proof of a model.) We treat quark and lepton chiral multiplets in the third generation and Higgs chiral multiplets as fundamental fields and hence their scalar bosons have soft SUSY-breaking masses of order of the gravitino mass, $m_{3/2}$, at the cut-off scale Λ ².

¹It is very interesting that two light generations in an $SO(10)$ GUT are naturally accommodated in $E_7/SO(10) \times U(1)$ ². It has been shown that if one eliminates the $U(1)$ ² in the unbroken subgroup one can couple the non-linear sigma model to supergravity without any explicit breaking of the E_7 [7]. We will discuss the E_7 model in a separate paper.

²The boundary condition of SUSY-breaking masses in the present paper may be also realized in a brane

2 An example of a non-compact manifold for the first and second generations

In defining a supersymmetric non-linear sigma model, it is not sufficient to specify a symmetry breaking $G \rightarrow H$. While this determines the number of Nambu-Goldstone (NG) bosons, the number of NG chiral multiplets is not uniquely determined [5, 6]. Consider the simple example of the $SU(2)/U(1)$ non-linear sigma model. This manifold is parameterized by two massless NG bosons, x_1 and x_2 . We may introduce two chiral multiplets, ϕ_1 and ϕ_2 , each of which contains one NG boson and one additional real, massless scalar. This realization is referred to as “doubled.” In this scenario, there are two charge eigenstates,

$$\phi_+ = \phi_1 + \phi_2, \quad \phi_- = \phi_1 - \phi_2, \quad (1)$$

which form a real representation of the unbroken subgroup. This is a general and unacceptable feature of the doubled realization because the standard model is chiral.

In the fully non-doubled or “pure” realization, the two true NG bosons lie in a single NG chiral multiplet, ϕ^+ . In this case, the ϕ^- is absent and the NG chiral multiplet ϕ^+ is a complex representation of the unbroken $U(1)$ subgroup. The resultant manifold is nothing but CP^1 . Unfortunately, it became known that the pure realization cannot be coupled to supergravity [4]. However, it has been recently pointed out that a hybrid realization with some doubled and some non-doubled NG multiplets does not suffer from this inconsistency [7]. We will therefore search for a hybrid non-linear sigma model that contains two generations of quarks and leptons as NG chiral multiplets.

Let us first consider a non-compact complex manifold that accommodates one generation of left-handed quark and lepton multiplets. In particular, take a SUSY $U(6)/[U(4) \times SU(2)]$ non-linear sigma model which consists of $(4 \times 2 + 1)$ NG chiral multiplets, ϕ_i^a and φ , where $a = 1, \dots, 4$ and $i = 1, 2$. The former superfield contains the left-handed quarks and leptons,

$$\phi_i^a = \begin{pmatrix} u_L^\xi & \nu_L \\ d_L^\xi & e_L^- \end{pmatrix} \sim (\mathbf{4}, \mathbf{2}) \quad (2)$$

world. That is, one assumes that quark and lepton multiplets in the first and second generation are confined on one brane separated from the other brane on which the third-generation quark and lepton, Higgs and hidden-sector multiplets reside. The gauge multiplets are in the bulk. This model may generate a partially realized Higgs-exempt [8] no-scale type supergravity model [9] where squarks and sleptons in the first and second generation have very small SUSY-breaking masses, while those in the third generation have masses of order the gravitino mass $m_{3/2}$.

where $\xi = 1, 2, 3$ is the color index. The latter is a non-standard-model field known as the “novino” [2]. All the bosons in ϕ_i^a and one real boson in φ are NG-boson coordinates of the $U(6)/[U(4) \times SU(2)]$ manifold. The other extra real boson in the novino superfield, φ , is necessary to construct the SUSY $U(6)/[U(4) \times SU(2)]$ non-linear sigma model [5]. Then, we have a complex manifold which consists of all 18 bosons.

We arrange these into a matrix,

$$\Psi = \begin{pmatrix} e^{\kappa\varphi/v} \mathbf{1}_2 \\ \phi_i^a/v \end{pmatrix}, \quad (3)$$

which has 12 components Ψ_i^α , $\alpha = 1, \dots, 6$. The general form of the Kähler potential of the SUSY $U(6)/[U(4) \times SU(2)]$ non-linear sigma model is then given by [10]

$$K = v^2 F(\det[\Psi_\alpha^\dagger \Psi^\alpha]), \quad (4)$$

where the dimension-one constant v is determined, together with the constant κ , by normalization conditions for the NG chiral multiplets as

$$v^2 \frac{\partial^2 F}{\partial \phi_a^{\dagger i} \partial \phi_j^b} \Big|_{\phi_i^a = \varphi = 0} = \delta_b^a \delta_i^j \quad (5)$$

$$(\kappa v)^2 \frac{\partial^2 F}{\partial \varphi^\dagger \partial \varphi} \Big|_{\phi_i^a = \varphi = 0} = 1. \quad (6)$$

The parameter v corresponds to the energy scale of the $U(6)$ breaking. Here, notice that the function $F(x)$ is an arbitrary function satisfying (5) and (6). This freedom originates from the presence of one extra (non-NG) boson in the novino superfield, φ [2, 6].

The above Kähler potential is invariant under the $U(6)_{\text{global}} \times SU(2)_{\text{local}}$ symmetry

$$\Psi \rightarrow g \Psi h^{-1}(x, \theta), \quad (7)$$

where g is a parameter of the global $U(6)$ transformation and $h(x, \theta)$ is a chiral superfield parameter of the hidden local $SU(2)$ transformation. The form in (4) is maintained by using the local $SU(2)$ transformation. Thus, the global $U(6)$ symmetry is non-linearly realized by the NG chiral multiplets, ϕ_i^a and φ .

Let us now couple the above model to supergravity. The interaction is given by

$$\Delta \mathcal{L} = 3 \int d^2\theta d^2\bar{\theta} \mathcal{E} \exp\left(\frac{1}{3} K(\phi_i^a, \varphi, \phi_a^{\dagger i}, \varphi^\dagger)\right). \quad (8)$$

Here, \mathcal{E} is the supervierbein determinant. It should be stressed here that the supergravity Lagrangian is completely invariant under the global $U(6)$ symmetry.

It is straightforward to introduce the hidden sector responsible for the SUSY breaking. For simplicity, we introduce a single singlet field, Z , for this purpose. Then, the total Kähler potential is

$$K = K(\phi_i^a, \varphi, \phi_a^{\dagger i}, \varphi^\dagger) + Z^\dagger Z + \dots \quad (9)$$

The introduction of this SUSY-breaking sector preserves the global $U(6)$ symmetry and, therefore, leaves our NG bosons massless. However, there is a real scalar in φ that is not a NG boson, and it acquires a soft mass of $\mathcal{O}(m_{3/2})$. This fact is shown by an explicit calculation [11].

So far, only the left-handed quarks and leptons have been introduced in our non-linear sigma model. It is straightforward to accommodate the right-handed quarks and leptons in another $U(6)/[U(4) \times SU(2)]$ manifold. The NG chiral multiplets are

$$\tilde{\Psi} = \begin{pmatrix} e^{\kappa\tilde{\varphi}/v} \mathbf{1}_2 \\ \tilde{\phi}_a^i/v \end{pmatrix}, \quad (10)$$

where the $\tilde{\phi}_a^i$ are the chiral multiplets for the right-handed quarks and leptons and the $\tilde{\varphi}$ is another novino. The total manifold is now $(U(6)/[U(4) \times SU(2)])^2$. The SM gauge group is a subgroup of the unbroken $(U(4) \times SU(2))^2$. If one gauges the $SU(2) \times SU(2)$ and a diagonal $SU(4)$ subgroup of the $U(4) \times U(4)$ in the unbroken symmetry, one obtains the Pati-Salam gauge model with one generation.

It is now clear how to extend the model to accommodate the second generation of quarks and leptons. That is, we consider a manifold $(U(10)/[U(8) \times SU(2)])^2$, such that the left and right multiplets are

$$(\phi_i^a)_L = \begin{pmatrix} u_L^\xi & \nu_{eL} & c_L^\xi & \nu_{\mu L} \\ d_L^\xi & e_L^- & s_L^\xi & \mu_L^- \end{pmatrix} \sim (\mathbf{8}, \mathbf{2}) \quad (11)$$

$$(\phi_i^a)_R = \begin{pmatrix} u_R^\xi & \nu_{eR} & c_R^\xi & \nu_{\mu R} \\ d_R^\xi & e_R^- & s_R^\xi & \mu_R^- \end{pmatrix} \sim (\mathbf{8}, \mathbf{2}). \quad (12)$$

Gauging suitable subgroups properly we obtain the supersymmetric standard model (SSM) with three generations, where the first two generations are Nambu-Goldstone bosons in the coset space and the third generation is fundamental. After SUSY breaking, according to the low-energy theorem we have massless squarks and sleptons in the first two generations. On

the other hand, the Higgs and the squarks and sleptons in the third generation may have soft-SUSY breaking masses of $\mathcal{O}(m_{3/2})$, since they are fundamental. The top Yukawa is also put in by hand, and given the non-degeneracy of the families, it breaks no symmetry and so is naturally taken to be $\mathcal{O}(1)$ [12].

The absence of Yukawa interactions along with the masslessness of squarks and sleptons in the first and second generations is guaranteed when the global $U(10) \times U(10)$ symmetry is exact. However, once we introduce the SSM gauge interactions the global symmetry is explicitly broken and the squarks and sleptons are no longer true NG bosons. Therefore, they may now appear in Yukawa interactions, but the Yukawa couplings are still suppressed. This is because the NG boson description remains approximately valid, since the global symmetry is only weakly gauged. After SUSY breaking, the radiative corrections from the gauge and Yukawa interactions induce small masses for the squarks and sleptons.

The induced masses are logarithmically divergent and hence we need counter terms in the Kähler potential. In principle, we cannot determine the counter terms, but we expect those terms to vanish at some cut-off scale Λ where the present non-linear sigma model is realized. In the present paper, we simply assume the GUT scale $\simeq 2 \times 10^{16}$ GeV to be the cut-off scale. In other words, we choose a boundary condition such that squarks and sleptons in the first and second generations are massless at the GUT scale. We easily see that squarks and sleptons in the first two generations have almost flavor-independent masses, since the SM gauge interactions are flavor blind and the Yukawa couplings are negligible compared with the gauge interactions. Thus, we do not have the serious flavor-changing neutral current problem.

However, this model does likely suffer from a gravitino problem [13] since $m_{3/2}$ is of $\mathcal{O}(1 \text{ TeV})$. The problem of late-decaying, non-LSP gravitinos can be solved through a dilution process with a sufficiently low reheating temperature [14], but such a discussion is beyond the scope of this paper. Similarly, although the novino may have interesting phenomenology because its mass is of $\mathcal{O}(m_{3/2})$, making numerical predictions would require an explicit model which we do not provide here.

The results that follow do not rely on any particular model. We assume that non-MSSM fields, including those of the GUT and the novino, are efficiently decoupled. Our results then follow from a set of SUSY-breaking parameters specified at the cut-off scale which are

generic to the NG hypothesis on non-compact manifolds.

3 Low-energy spectrum for SUSY particles

Consistent with the NG hypothesis on non-compact manifolds, we consider the subspace of mSUGRA [15] models with the SUSY-breaking parameters

$$m_{1/2} = 300 \text{ GeV}, \quad \tan \beta = 10, \quad \mu > 0, \quad A_0 = 0 \quad (13)$$

while setting $m_0 = 0$ for the first and second generation of scalars and $m_0 = 1 \text{ TeV}$ for the third generation scalars. Using the **SOFTSUSY** SUSY spectrum calculator (version 3.0.7) [16] and the **DarkSUSY** suite (version 5.0.5) [17, 18, 19, 20] we scan the (M_{H_u}, M_{H_d}) parameter space where $M_{H_u} \sim M_{H_d} \sim \mathcal{O}(m_{3/2})$ to find the region which gives the correct dark matter relic density while also evading other phenomenological constraints. We set the top mass to $m_t = 175 \text{ GeV}$ and let **SOFTSUSY** solve for the GUT scale, which is always $\simeq 2 \times 10^{16} \text{ GeV}$. Results for the most relevant bounds are shown in Figure 1. The colored regions are as follows:

- **red:** 3σ -allowed dark matter relic density given by the seven-year WMAP data [21].
- **gray:** Charged LSP.
- **magenta:** Excluded by **DarkSUSY** limits on $b \rightarrow s\gamma$.
- **yellow:** Excluded by **DarkSUSY** Higgs mass bounds.
- **blue:** Excluded by 90% limit on spin-independent WIMP–nucleon cross sections in direct detection experiments [22].
- **green:** Excluded by 90% limit on spin-*dependent* WIMP–nucleon cross-sections in direct detection experiments [22]. For any given bin the more stringent limit among the proton or neutron cross-sections is chosen.

The allowed parameter space in Figure 1 shows some interesting properties. First, significantly different combinations of (M_{H_u}, M_{H_d}) can give the correct relic density. In the upper and lower “branch” regions with a large difference between the two soft masses, coannihilation with \tilde{e} , $\tilde{\mu}$ or $\tilde{\nu}_{e,\mu}$ yields the required abundance. The “bridge” at $M_{H_u} \approx M_{H_d} \approx$

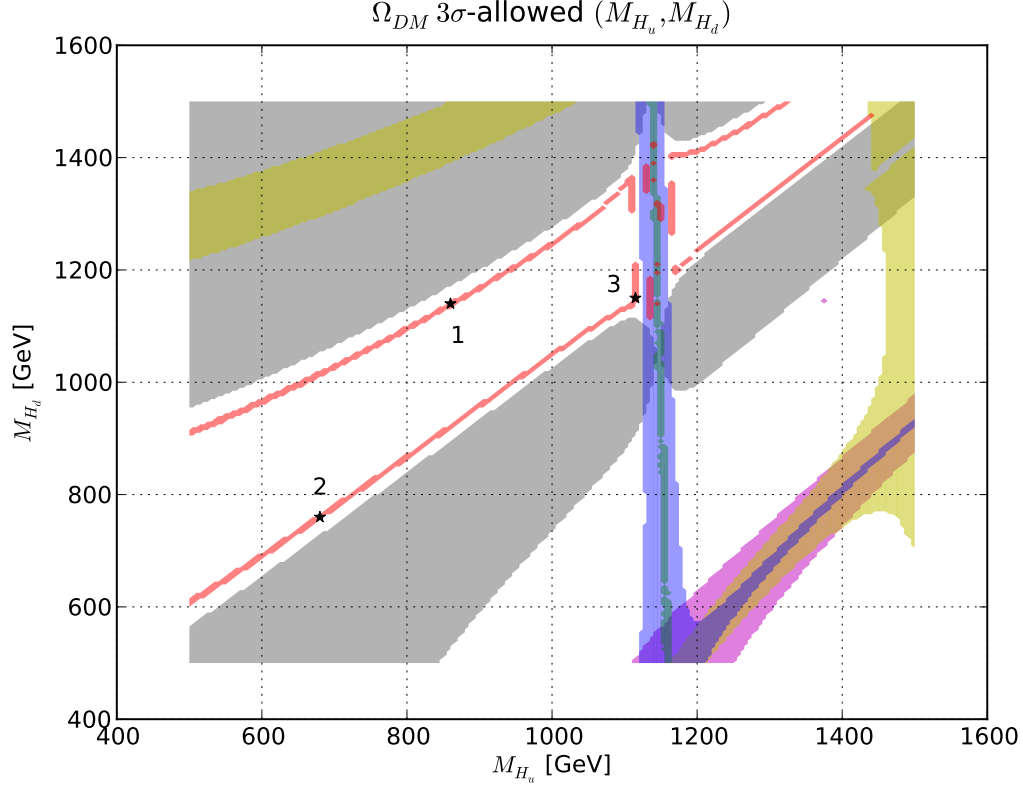


Figure 1: Scan in (M_{H_u}, M_{H_d}) for the non-universal mSUGRA subspace $m_{1/2} = 300$ GeV, $\tan \beta = 10$, $\mu > 0$ and $A_0 = 0$, with $m_0 = 0$ for the first and second generation scalars and $m_0 = 1$ TeV for the third generation scalars. The regions shown are: 3σ -allowed dark matter relic density given by the seven-year WMAP data (red), charged LSP (gray), excluded by **DarkSUSY** limits on $b \rightarrow s\gamma$ (magenta), excluded by **DarkSUSY** Higgs mass bounds (yellow), excluded by 90% limit on spin-independent WIMP-nucleon cross sections in direct detection experiments (blue), excluded by 90% limit on spin-dependent WIMP-nucleon cross sections in direct detection experiments (green). Benchmark points chosen for further study are denoted by the black stars (see text for details).

1100 GeV is a small- μ region where annihilation through \tilde{h} contributes to the correct abundance for a relatively light neutralino [23]. Due to the large higgsino component in $\tilde{\chi}_1^0$, this bridge branch is near the region excluded by direct detection experiments (see, for example, Ref. [24]). For the upper, lower and bridge branches we have chosen benchmark points for further study, marked by black stars. (These benchmark points give dark matter relic densities within 1σ of the WMAP7 value.)

Second, the regions giving the correct relic density are far from those excluded by bounds from $b \rightarrow s\gamma$ and Higgs mass. The former is not surprising since we have chosen small $\tan\beta$, $\mu > 0$ and a gaugino soft mass that is not too light, but heavy \tilde{t} and \tilde{b} also suppress the relevant diagrams. If \tilde{t} and \tilde{b} were nearly as light as the squarks of the first and second generation, the $b \rightarrow s\gamma$ limit would be exceeded for nearly all of the (M_{H_u}, M_{H_d}) plane. Similarly, the Higgs mass bound is also avoided rather easily because \tilde{t} is heavy, enhancing the contribution of the y_t term in the MSSM running of the h_0 mass, although the relationship to (M_{H_u}, M_{H_d}) is more intricate. For comparison, see Figure 2, which has the same parameters as Figure 1 except that $m_0 = 0$ for the third generation scalars as well.

Finally, we note that at small m_0 a gaugino soft mass $m_{1/2} \simeq 300$ has some phenomenological support, as it gives $\tilde{\chi}_{1,2}^0$ and $\tilde{\chi}_{1,2}^\pm$ masses favored by muon $g - 2$ [25]. Also, although a small m_0 usually gives dangerously small $\tilde{\tau}$ masses [25], this is not the case if it is only for the first and second generations. This accounts for the difference between the gray regions of Figures 1 and 2.

Altogether, these properties show that for the choices $\tan\beta = 10$, $\mu > 0$ and $A_0 = 0$, the NG hypothesis meets the relevant SUSY phenomenological requirements rather generically: several different regions of (M_{H_u}, M_{H_d}) at the correct mass scale can give the required relic density, and only a small portion of these regions is subject to other phenomenological constraints. This is consistent with previous work which found that SUSY phenomenological requirements can be satisfied by mSUGRA with a sufficiently heavy third generation, albeit with equal M_{H_u} and M_{H_d} [26].

We now consider how this scenario can be distinguished from conventional mSUGRA by examining the spectra of the benchmark points, whose (M_{H_u}, M_{H_d}) are shown in Table 1.

First, we choose a conventional mSUGRA point with similar soft masses for comparison:

$$m_0 = 75 \text{ GeV}, \quad m_{1/2} = 300 \text{ GeV}, \quad \tan\beta = 10, \quad \mu > 0, \quad A_0 = -200 \text{ GeV}. \quad (14)$$

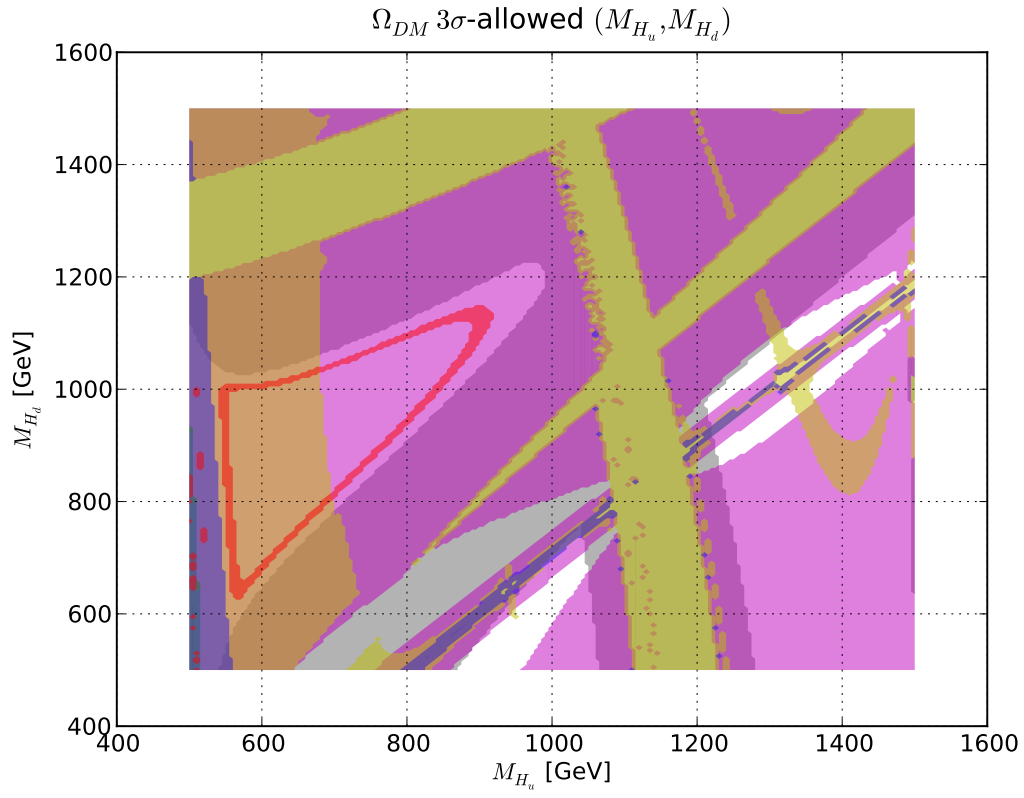


Figure 2: Same as Figure 1, except with $m_0 = 0$ for the third generation scalars as well.

Benchmark point	M_{H_u}	M_{H_d}
BP 1	860	1140
BP 2	680	760
BP 3	1115	1150

Table 1: Higgs soft masses for benchmark points, in GeV.

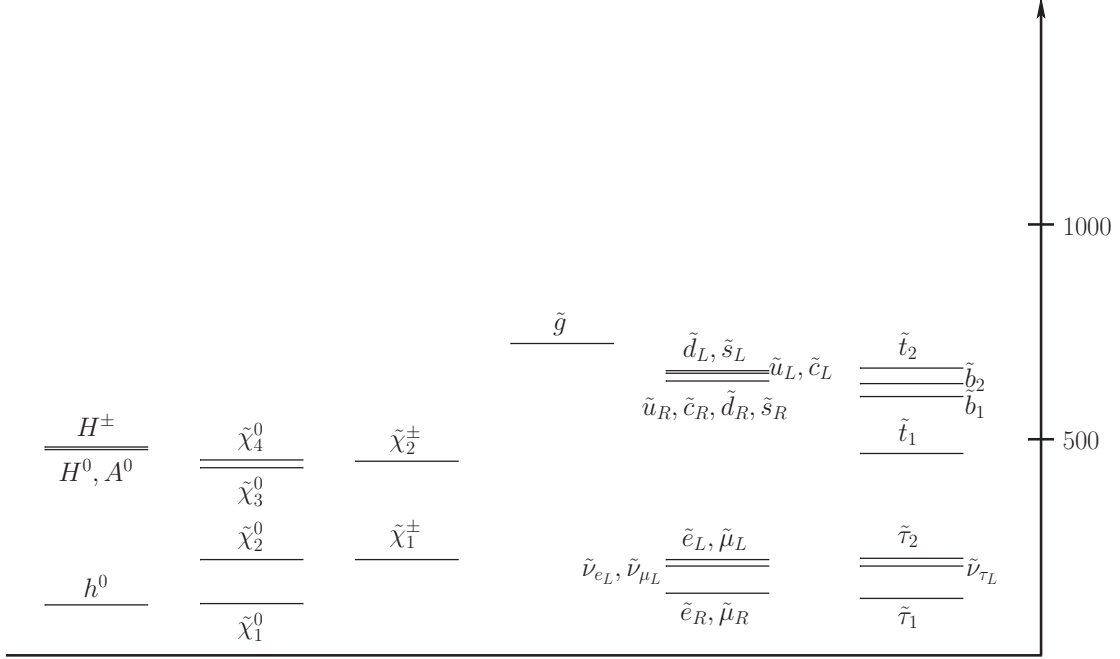


Figure 3: Spectrum for comparison point (CP), in GeV.

This point, denoted CP, gives roughly the correct $\tilde{\chi}_1^0$ relic density through $\tilde{\tau}$ coannihilation and exhibits a small \tilde{l}_R - $\tilde{\chi}_1^0$ mass splitting. The choice of $A_0 = -200$ GeV is to avoid Higgs mass bounds. The resulting spectrum is shown pictorially in Figure 3. (A complete numerical listing of masses is given in Table 6 of the Appendix, which starts on 25.)

Let us consider benchmark point 1 (BP 1) shown in Figure 4. As expected, compared to CP, the third generation scalars are very heavy, as are the heavy Higgs bosons due to the large values of M_{H_u} and M_{H_d} . Also, like CP, there is a small splitting between the lightest slepton and $\tilde{\chi}_1^0$. However, the expected hierarchy of sleptons is “inverted,” i.e. $\tilde{\nu}_{e,\mu}$ and \tilde{e}_L are lighter than \tilde{l}_R . This is due to the S term in the running of the scalar masses (see, for example, Ref. [27]),

$$16\pi^2 \frac{d}{dt} m_{\phi_i}^2 = - \sum_a 8C_a(i) g_a^2 |M_a|^2 + \frac{6}{5} Y_i g_1^2 S \quad (15)$$

where

$$S \equiv \text{Tr} [Y_j m_{\phi_j}^2] = M_{H_u}^2 - M_{H_d}^2 + \text{Tr} [\mathbf{m}_{\mathbf{Q}}^2 - \mathbf{m}_{\mathbf{L}}^2 - 2\mathbf{m}_{\mathbf{u}}^2 + \mathbf{m}_{\mathbf{d}}^2 + \mathbf{m}_{\mathbf{e}}^2] . \quad (16)$$

In (16), the rightmost trace is zero for our case since m_0 is universal across all the scalars in a given generation, so $S = (M_{H_u}^2 - M_{H_d}^2)$. Since \tilde{l}_R^* has hypercharge of $Y = +1$, but \tilde{l}_L and

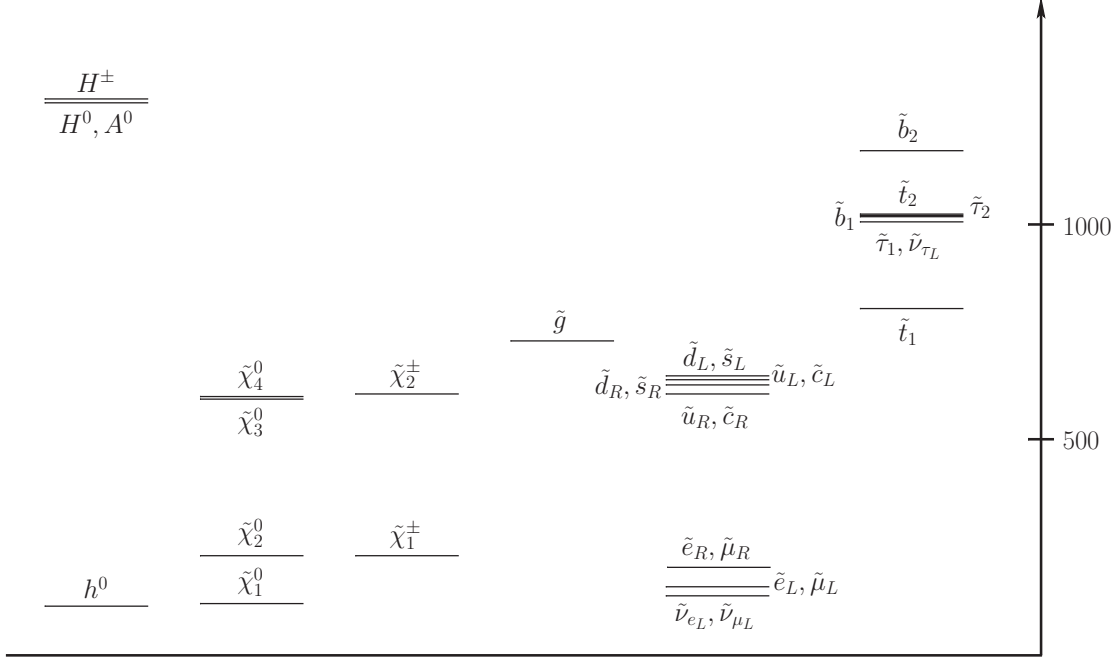


Figure 4: Spectrum for benchmark point 1 (BP 1), in GeV.

$\tilde{\nu}_{e,\mu}$ have hypercharge of $Y = -1/2$, \tilde{l}_R is driven heavier. For the same reason, the spectrum of the left and right squarks of the first and second generations is brought closer together than in CP. Unfortunately, the size of this effect is difficult to estimate analytically since M_{H_u} and M_{H_d} are themselves subject to significant running due to S .

Benchmark point 2 (BP 2) in Figure 5 is similar to BP 1, except that $(M_{H_u}^2 - M_{H_d}^2)$ is smaller, so the slepton hierarchy is narrowed but remains non-inverted. Benchmark point 3 (BP 3) in Figure 6 is also similar, with $(M_{H_u}^2 - M_{H_d}^2)$ being even smaller. Except, in addition to a non-inverted and narrowed slepton hierarchy, because it is in the bridge branch it exhibits typical small- μ neutralino and chargino hierarchies. In fact, $\tilde{\chi}_2^0$ and $\tilde{\chi}_1^\pm$ are lighter than $\tilde{\nu}_{e,\mu}$, closing off that decay channel.

In the next section, we discuss how these points can be identified at a collider, and use simulated events to demonstrate that this can be done early in 14 TeV running at the LHC.

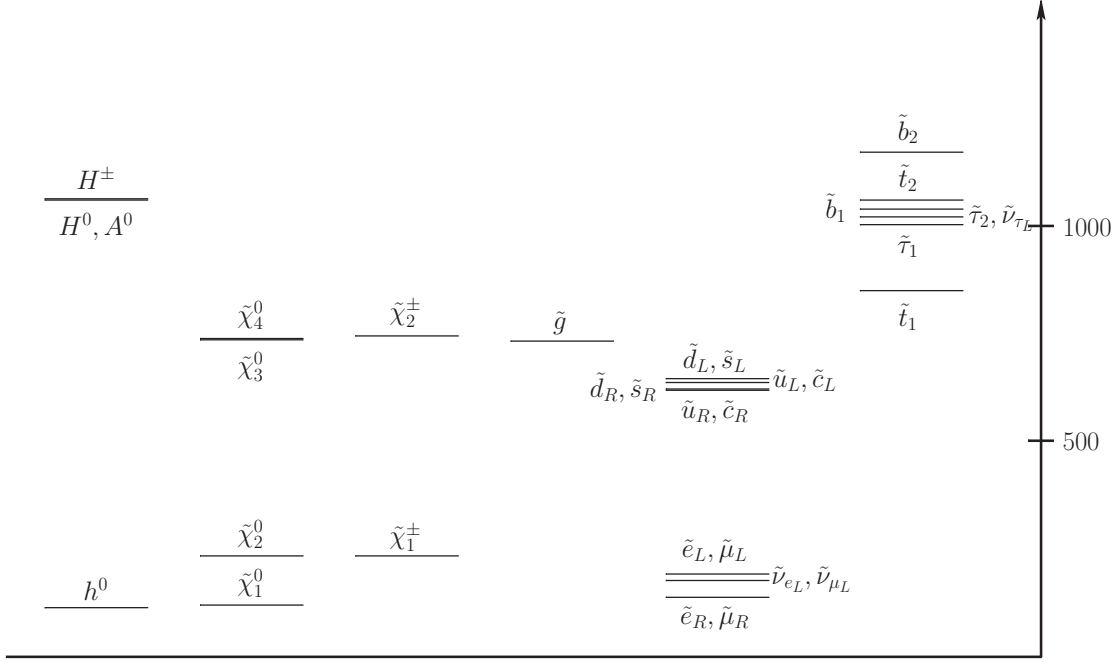


Figure 5: Spectrum for benchmark point 2 (BP 2), in GeV.

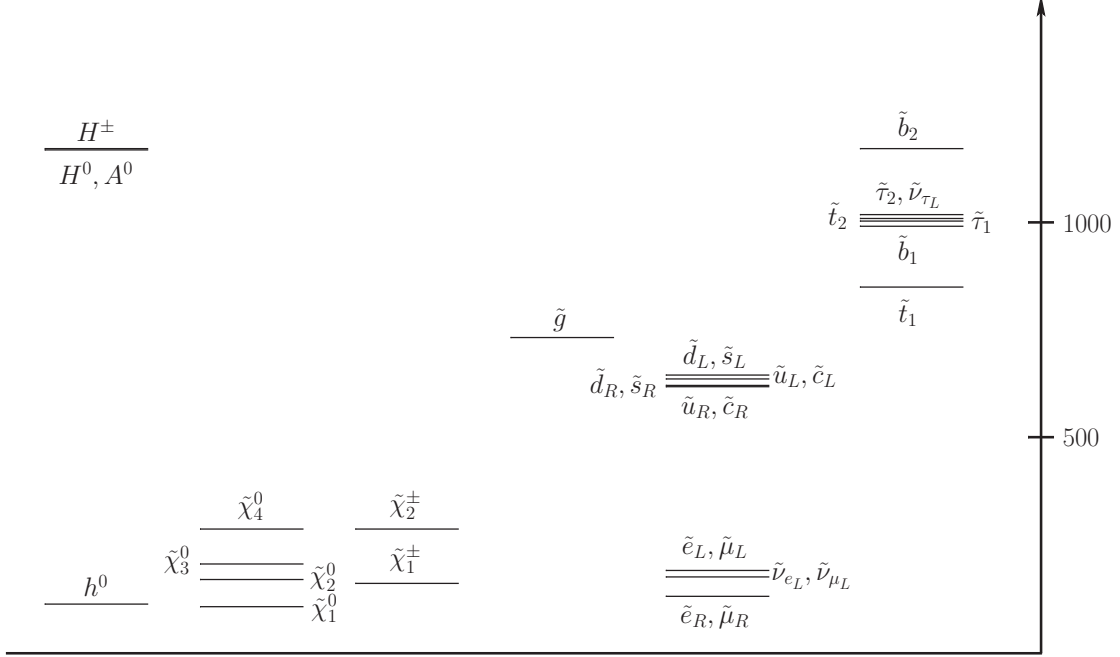


Figure 6: Spectrum for benchmark point 3 (BP 3), in GeV.

$m_{1/2}$ GeV	$m_3 = m_{1/2} \times 0.7$	$\times 1$	$\times 1.3$
300	27.9	13.0	1.8
400	31.5	18.2	3.2
500	33.5	20.9	7.8

Table 2: Branching ratios (%) for \tilde{g} decaying into b -jets for various $m_{1/2}$ and m_3 .

4 LHC physics

4.1 Discrimination at the LHC

We now consider the distinguishing characteristics of NG hypothesis model points and their prospects for detection at the LHC.

Under the NG hypothesis, m_3 (i.e., m_0 for the third generation) is of a much higher order than m_0 for the first and second generations. Therefore, the third generation scalars are significantly heavier than the squarks of the first and second generations. On the other hand, the relationship between $m_{1/2}$ and m_3 is not established by the model. While we have chosen $m_3 = 1$ TeV, the value could be much smaller, so the mass ordering between \tilde{g} and the third generation scalars is not fixed. Consequently, the multiplicity of b -jets from gluino production is sensitive to the value of m_3 .

To study the effect of this uncertainty, in Table 4.1 we list the branching ratios (%) of gluinos decaying into modes with b -jets for $m_{1/2} = 300, 400$ and 500 GeV. For $m_3 = 0.7 m_{1/2}$ the branching ratio is around 30% because the decays are fully open. However, if $m_3 = 1.3 m_{1/2}$, the branching ratio is less than 1/4 of the $m_3 = 0.7 m_{1/2}$ case. At our choice of $m_{1/2} = 300$ GeV and $m_3 = 1$ TeV the branching ratio is only $\mathcal{O}(1\%)$. By contrast, because the gaugino mass correction is smaller for slepton masses, the scalar mass of the order of gaugino mass at GUT scale is enough to make the third generation slepton heavier than the second lightest neutralino. Therefore, $\tilde{\tau}$ would not be produced in neutralino and chargino decays irrespective of the value of m_3 . Consequently, few τ -jets would be observed at the LHC, regardless of the relationship between the $m_{1/2}$ and m_3 .

Turning to leptons, because $\tilde{\chi}_2^0 \rightarrow \tilde{\tau}\tau$ is closed, there will be many more events with the number of leptons $n_l \geq 2$ than for conventional mSUGRA points. In the bridge branch, $\tilde{\chi}_2^0 \rightarrow \tilde{\nu}_{e,\mu}\nu_{e,\mu}$ is closed as well, and $\tilde{q} \rightarrow q\tilde{\chi}_4^0$ and $\tilde{q}_L \rightarrow q_L\tilde{\chi}_2^\pm$ are open due to gaugino mixing

caused by small μ ; however, most importantly, the right squarks have a large branching ratio to $\tilde{\chi}_2^0$ due to bino mixing. Thus for BP 3 the number of $n_l \geq 2$ events is greatly enhanced, even over BP 1 and BP 2. Overall, NG hypothesis model points require less integrated luminosity than conventional points in order to reconstruct two-lepton decay chains.

In short, τ -jet and lepton multiplicities can broadly distinguish NG hypothesis model points from conventional model points. Moreover, a lack of b -jets would support the hypothesis, but a normal multiplicity of b -jets would not falsify it.

For greater precision, the effects of the S -term on the slepton mass hierarchy should be visible at the LHC. At BP 1 and BP 2, the left squarks will decay mostly to $q_L \tilde{\chi}_2^0$ and $q_L \tilde{\chi}_1^\pm$ because these gauginos are mostly wino, and these in turn will decay mostly into left sleptons. The right squarks will decay mostly to $q_R \tilde{\chi}_1^0$ because $\tilde{\chi}_1^0$ is mostly bino, so no leptons will be produced. Thus, at these points we expect the leptons produced in the squark decay chain $\tilde{q} \rightarrow \chi_2^0 q \rightarrow q \tilde{l}^\pm l^\mp$ to be mostly left-handed. By comparison, at CP $\tilde{\chi}_2^0 \rightarrow \tilde{l}_R^\pm l^\mp$ exclusively since \tilde{l}_L is too heavy — most of these leptons will be right-handed.

Because the chirality of the lepton is fixed by the interaction vertex, the direction of the lepton in the rest frame of the squark is correlated with the quark and lepton chirality. Namely, for the final states $q_L l_L$ ($q_R l_R$, $q_L \bar{l}_R$, $q_R \bar{l}_L$) the jet and lepton tend to go to in opposite directions while for the $q_L l_R$ ($q_R l_L$, $q_L \bar{l}_L$, $q_R \bar{l}_R$) final state they tend to go in the same direction. Since the LHC is a p - p collider, more \tilde{q} is produced than \tilde{q}^* , so there will be a charge asymmetry in the distribution of the jet-lepton invariant mass. The lepton from the slepton decay is not correlated since the slepton is scalar. Then, for BP 1 and BP 2, there will be a large charge asymmetry since most of the $\tilde{\chi}_2^0$ are from \tilde{q}_L rather than \tilde{q}_R , and $\tilde{\chi}_2^0$ decays predominantly to $\tilde{l}_L l_L$. Note that the charge asymmetry is opposite for CP because here the dominant channel is $\tilde{q}_L \rightarrow \tilde{\chi}_2^0 \rightarrow \tilde{l}_R$.

The situation is more complicated at BP 3 because so many different squark decay channels are open. Moreover, because $\tilde{\chi}_2^0$ is so light, it can only decay to \tilde{l}_R . We first observe that the right squarks produce leptons mostly through $\tilde{\chi}_2^0$ (22%) with a lower branching fraction than left squarks (17% for up, 10% for down). The charge asymmetry from right squarks is that of $\tilde{q}_R \rightarrow \tilde{\chi}_2^0 \rightarrow \tilde{l}_R$, the same sign as BP 1 and BP 2, but not as large. To clearly distinguish BP 3 from BP 1 and BP 2, its small- μ character can be seen by observing the tight neutralino mass hierarchy through the small $\tilde{\chi}_2^0$ - $\tilde{\chi}_1^0$ mass splitting. In addition, the

decay of squarks to heavier neutralinos can be observed. For example, \tilde{q}_L decay into $\tilde{\chi}_4^0$ and $\tilde{\chi}_{1,2}^\pm$ with branching ratios 15% and 65%, respectively.

Lastly, at all the benchmark points the heavy states in the Higgs sector will not be produced in sufficient quantities to be identified because their mass is too high. However, if $\tan\beta > 15$, a heavy Higgs of $\mathcal{O}(500 \text{ GeV})$ may be observed at a CP-like model point [29].

4.2 Simulation and reconstruction

To demonstrate this phenomenology at the LHC, for each of the model points we generated 10^5 signal events at 14 TeV for inclusive squark production using the **ISAJET** (version 7.72) spectrum calculator [30], **HERWIG** (version 6.5) shower generator [31] and **AcerDET** (version 1.0) [32] fast detector simulation. (MSSM input parameters were tuned slightly such that **ISAJET** would produce the same spectrum as **SOFTSUSY**.) The inclusive production cross section is $\gtrsim 15 \text{ pb}$, so the integrated luminosity required for the following analysis is only 7 fb^{-1} ; this should be achievable in roughly one month of running [33].

To grossly distinguish NG hypothesis model points from conventional points we first extract and compare:

- number of b -jets n_b with $p_T > 50 \text{ GeV}$
- number of τ -jets n_τ with $p_T > 20 \text{ GeV}$
- number of leptons n_l with $p_T > 15 \text{ GeV}$ and $\eta < 2$.

Here, the b - and τ -jets are the jets labeled as such³ by **AcerDET**, with an efficiency of around 80%. However, real tagging efficiencies are probably around 60% and 50% for b - and τ -jets, respectively [32]. The results are shown in Table 3, as a percentage of events. As expected, for the benchmark points there are a few b -jets and very few τ -jets from direct production of third generation squarks. BP 3 shows an enhancement in τ -jets from off-shell $\tilde{\chi}_1^\pm$ decays via the W boson. By contrast, CP has many b -jets from both gluino and third generation squark decays, as well as many τ -jets (and therefore fewer multi-leptons) from $\tilde{\chi}_2^0$ decays.

Turning to the other discriminators, in order to obtain the $\tilde{\chi}-\tilde{l}$ mass splittings and charge

³Only hadronic τ decays passing certain cuts are labeled as τ -jets by **AcerDET**. Thus, leptonic τ decays are not included in n_τ . See the **AcerDET** manual [32] for details.

Model point	% $n_b \geq 1$	% $n_\tau \geq 1$	% $n_l \geq 2$
BP 1	2.29	0.04	15.80
BP 2	2.22	0.02	15.84
BP 3	3.17	2.284	28.97
CP	31.70	16.94	4.10

Table 3: Percentage of events with the given multiplicities (see text for details).

asymmetry, we must study the gluino and squark decay chains

$$(\tilde{g} \rightarrow) \tilde{q}(j) \rightarrow \tilde{\chi}_2^0 jj \rightarrow \tilde{l}^\pm jj l_1^\mp \rightarrow jj l_1^\mp l_2^\pm + \cancel{E}_T. \quad (17)$$

Henceforth, we define the lepton l_1^\mp from $\tilde{\chi}_2^0$ decay as the “near” lepton, and the lepton l_2^\pm from \tilde{l} decay to be the “far” lepton. We use the method of invariant mass distributions and endpoints to reconstruct the masses [29, 34, 35]. Here, one creates distributions of the invariant masses $m_{p_1 p_2 \dots}$ of the final state particles, then identifies the upper endpoint of each distribution $m_{p_1 p_2 \dots}^{max}$. These endpoint values are then inverted to obtain the masses of the particles in the decay chain. We use the following invariant masses in our reconstruction:

- m_{ll} , the invariant mass of both leptons
- m_{jll} , the invariant mass of both leptons + the jet from squark decay
- $m_{jl(lo)} \equiv \min(m_{jl_1}, m_{jl_2})$, where each m_{jl_i} is the invariant mass of the jet from squark decay and one of the leptons
- $m_{jl(hi)} \equiv \max(m_{jl_1}, m_{jl_2})$.

This method can determine the $\tilde{l}-\tilde{\chi}_1^0$ and $\tilde{\chi}_2^0-\tilde{l}$ mass splittings rather precisely, which is useful here; extracting the squark mass scale is less critical because it is mostly determined by m_0 . We use the MINUIT2 fitter in ROOT [36] to find the endpoints, and the inversion formulas in Ref. [35] to find the mass differences and squark mass.

For each model point we identify events with $n_l \geq 2$, $n_j \geq 2$ where the two highest p_T leptons are same-flavor/opposite-sign (SFOS). To subtract the chargino contribution to SFOS, we also identify $n_l = 2$ events with different-flavor/opposite-sign (DFOS) and subtract these counts from the SFOS invariant mass distributions before fitting. In a given event, we choose the jet among the two highest p_T jets that gives the smallest m_{jll} . This identifies the jet from squark decay on the correct branch.

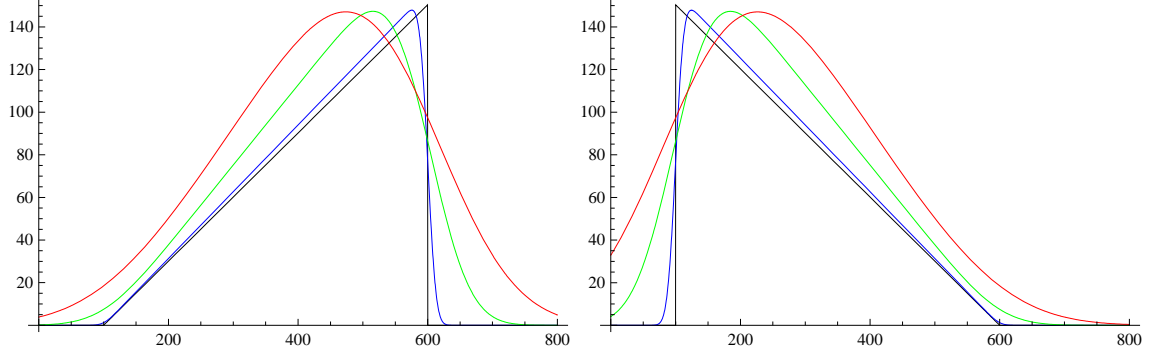


Figure 7: Example fitting functions with endpoint = 600 and gaussian smearing widths = 0 (black), 10 (blue), 50 (green) and 100 (red). On the left the endpoint shape is a vertical edge, whereas on the right it is a ramp.

Noting the example mass distribution shapes in Ref. [35], we use the vertical edge with gaussian smearing in order to fit the m_{ll}^{max} endpoint, and a ramp function with gaussian smearing in order to fit the m_{jll}^{max} and $m_{jl(lo)}^{max}$ endpoints (for examples showing both kinds of shapes, see Figure 7). We also choose a vertical edge for $m_{jl(hi)}$ because $m_{jl(near)}$ (the jet–near lepton invariant mass distribution) has edges. This is a good choice for the BP 1, BP 3 and CP because $m_{jl(near)}^{max} > m_{jl(far)}^{max}$. At point BP 2, $m_{jl(near)}^{max} < m_{jl(far)}^{max}$, so this endpoint shape does not provide a good fit. In this case, the $m_{jl(hi)}$ distribution is much closer in shape to a ramp function near the end point, and it has a discontinuity at $m_{jl(hi)} \sim m_{jl(lo)}^{max}$. We call this discontinuity a “secondary edge.” We try both the smeared ramp and a smeared vertical edge to fit this endpoint.

In our fits the smearing width is left as a free parameter to match the broadening of the endpoint due to energy uncertainty and other effects included in the simulation which reduce the number of events near the endpoint; this is most apparent in the $m_{jl(hi)}^{max}$ fits.

In addition, for BP 3, there are significant tails in the $m_{jl(hi)}$ and m_{jll} distributions due to the decays of $\tilde{\chi}_4^0$ and $\tilde{\chi}_2^\pm$. In these fits the fitting function is a smeared ramp added to a sloping line in piecewise fashion. Moreover, in these functions we set the maximum smearing width to 5 GeV and over a limited mass range to avoid over-fitting to the curves of the edges which are resolvable due to the large statistics.

The $\tilde{\chi}_4^0$ and $\tilde{\chi}_2^\pm$ edges of BP 3 can be seen in the m_{ll} mass distribution in Figure 8. At 93 GeV is the $\tilde{\chi}_2^\pm \rightarrow \tilde{\nu}_L l^\pm \rightarrow \tilde{\chi}_1^\pm ll$ endpoint, and at 107 GeV is the $\tilde{\chi}_4^0 \rightarrow \tilde{l}_L l \rightarrow \tilde{\chi}_2^0 ll$

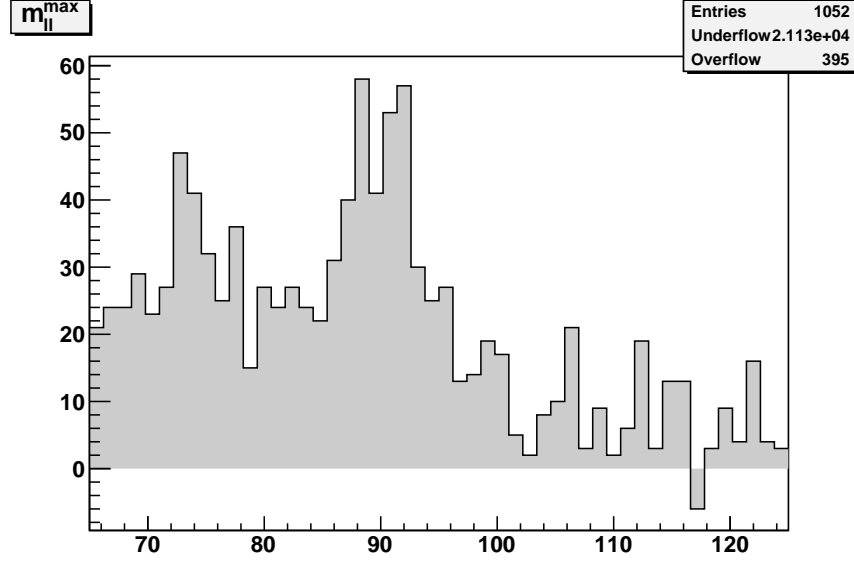


Figure 8: Higher range of m_{ll} for BP 3. At 93 GeV is the $\tilde{\chi}_2^\pm \rightarrow \tilde{\nu}_L l^\pm \rightarrow \tilde{\chi}_1^\pm ll$ endpoint, and at 107 GeV is the $\tilde{\chi}_4^0 \rightarrow \tilde{l}_L l \rightarrow \tilde{\chi}_2^0 ll$ endpoint.

Model point	$m_{\tilde{l}} - m_{\tilde{\chi}_1^0}$	$m_{\tilde{\chi}_2^0} - m_{\tilde{l}}$	$m_{\tilde{q}} - m_{\tilde{\chi}_2^0}$	$m_{\tilde{q}}$
BP 1	37.7 ± 1.1 (37.9)	73.3 ± 1.9 (73.5)	433 ± 7 (428)	655 ± 35 (660)
BP 2	72.9 ± 0.7 (73.5)	40.8 ± 0.3 (40.8)	414 ± 3 (409)	660 ± 10 (643)
BP 3	29.1 ± 1.0 (28.9)	31.4 ± 0.9 (31.6)	491 ± 12 (472)	693 ± 88 (639)
CP	27.7 ± 3.3 (25.7)	76.0 ± 4.5 (77.5)	497 ± 51 (444)	848 ± 237 (666)

Table 4: Reconstructed mass differences and squark masses, in GeV. True values are shown in parentheses.

endpoint. All the other plots of the mass distributions and their fit endpoints, as well as all the inversion solutions, are shown in the Appendix . In these plots the cross-hatched region shows the parton-level mass distributions, and the solid region the jet-level distributions. One observes that the fitting function identifies the m_{ll}^{max} endpoints correctly without any shifts. Also, one can see that the jet-level distributions have fewer counts in the bins near the endpoint and more counts in the lower energy bins. This is due to effects such as initial state radiation and jet misidentification.

Here, we show the correct solutions in Table 4, where the values in the parentheses are the true values. The correct solution is chosen by first noting that none of the model points have

Model point	$A_{c,soft}$	$A_{c,hard}$
BP 1	-0.11 ± 0.02	0.25 ± 0.02
BP 2	-0.04 ± 0.02	0.11 ± 0.02
BP 3	-0.01 ± 0.01	0.04 ± 0.01
CP	0.04 ± 0.04	-0.14 ± 0.06

Table 5: Lepton charge asymmetries for each model point.

off-shell decays in the squark decay chains, which would manifest in flat mass distributions. This eliminates Region 4 of m_{jll}^{max} , in the terminology of Ref. [35]. Next, among the Region 1 solutions we choose the one with the plausible squark mass that would give the observed production cross-section. If this is ambiguous, looking at the $m_{jl(hi)}$ mass distribution, if there is a secondary edge then the lepton at the fit edge is the far lepton, and so the $\tilde{l}-\tilde{\chi}_1^0$ splitting is larger than the $\tilde{\chi}_2^0-\tilde{l}$ splitting; conversely, if there is no secondary edge, the fit lepton is the near lepton, and the $\tilde{\chi}_2^0-\tilde{l}$ splitting is the larger one.

Finally, to calculate the charge asymmetry, we create $m_{jl\pm}$ distributions separately for both of leptons, where j is the same jet as from m_{jll} . This gives us four distributions $m_{jl\pm(soft)}$ and $m_{jl\pm(hard)}$ where the former distribution is for the lepton with the lower p_T of the two, and the latter is for the lepton with the greater p_T (these are also shown in the Appendix). Then, we integrate each of the distributions,

$$N(l) = \int_a^b dm' m_{jl}(m') \quad (18)$$

where $(a, b) = (m_{jl(lo)}^{max} - 100 \text{ GeV}, m_{jl(lo)}^{max})$ for the soft distribution. For the hard distribution, $(a, b) = (m_{jl(near)} - 100 \text{ GeV}, m_{jl(near)})$ where m_{near} is the edge of the $m_{jl(hi)}$ distribution for the near lepton. For our model points, $m_{jl(near)} \neq m_{jl(hi)}^{max}$ only for BP 2, which has a secondary edge at 350 GeV.

This gives us four quantities $N_{soft}(l^\pm)$ and $N_{hard}(l^\pm)$. Finally, we define the charge asymmetry⁴ as

$$A_c \equiv \frac{N(l^-) - N(l^+)}{N(l^-) + N(l^+)} . \quad (19)$$

The soft and hard lepton charge asymmetries, $A_{c,soft}$ and $A_{c,hard}$, are shown for each of the model points in Table 5. We see that $|A_{c,soft}| < |A_{c,hard}|$, since more of the soft leptons are from slepton decay.

⁴Our definition has the opposite sign from some others in the literature.

4.3 Model point identification

Using the results from the reconstruction procedures above, we describe how to identify the different model points from the data. We will assume universal gaugino soft masses at high scale, such that $M_3 : M_2 : M_1 \approx 6 : 2 : 1$ at low scale [27].

BP 1

The single edge of the $m_{jl(hi)}$ distribution suggests that this is from the near lepton. The large $\tilde{\chi}_2^0 - \tilde{\chi}_1^0$ mass splitting and non-observation of higher m_{ll} edges from $\tilde{\chi}_4^0$ and $\tilde{\chi}_2^\pm$ decays indicate that $\mu > M_2 - M_1$, so $\tilde{\chi}_2^0$ is gaugino-dominated and the decay chains are primarily from left squarks. Combined with the large positive (by our definition, Eq. 19) charge asymmetry, this suggests that the slepton for this edge is \tilde{l}_L . Following the mSUGRA mass relations [27], the large $\tilde{\chi}_2^0 - \tilde{l}_L$ splitting is inconsistent with mSUGRA assumptions; on the other hand, the $\tilde{l}_L - \tilde{\chi}_1^0$ splitting is small enough to give the correct dark matter relic abundance. Then, we can infer that \tilde{l}_R is heavier than \tilde{l}_L . Along with the lack of b - and τ -jets, an upper branch point in the NG hypothesis is a plausible candidate.

BP 2

Again, the $\tilde{\chi}_2^0 - \tilde{\chi}_1^0$ splitting is large and no higher m_{ll} edges are observed, so we are not in a small- μ region and left squark decays produce the most leptons. The secondary edge at 350 GeV in the $m_{jl(hi)}$ distribution suggests that the fitted edge is for the far lepton. Combined with the large $\tilde{l} - \tilde{\chi}_1^0$ mass splitting and positive charge asymmetry, we infer that this edge is for the \tilde{l}_L and that there is an unresolved \tilde{l}_R close to $\tilde{\chi}_1^0$, giving the correct dark matter relic abundance. The smaller charge asymmetry than for BP 1 is consistent with the far lepton being more likely to be the hard lepton, contributing roughly 50% below 350 GeV in the $m_{jl(hi)}$ distribution. Thus, in this case, a lower branch point in the NG hypothesis is a plausible candidate.

BP 3

The additional edges in the m_{ll} distribution due to the higher neutralinos and the small $\tilde{\chi}_2^0 - \tilde{\chi}_1^0$ mass splitting suggest a small- μ point. These edges can be reconstructed to obtain the masses of these heavy neutralinos [28]. Combining the inferred branching ratios, we can

determine that right squark decays contribute more strongly to the the charge asymmetry. Since the asymmetry is positive, this suggests that the reconstructed slepton is \tilde{l}_R ; we can reconstruct \tilde{l}_L and $\tilde{\nu}_L$ at some specific higher mass. A bridge branch point is consistent with all these features, as well as with the enhancement in the number of multi-lepton events over BP 1 and BP 2.

CP

Unlike the three scenarios above, here we observe a typical number of b - and τ -jets along with few multi-lepton events. Since the $\tilde{\chi}_2^0$ - $\tilde{\chi}_1^0$ splitting is large, this is not a small- μ point, so most of the multi-lepton events are from left squark decays. Combined with the negative charge asymmetry, we infer that the slepton for this edge is \tilde{l}_R . We also see that the lepton is near, so it is the $\tilde{\chi}_2^0$ - \tilde{l}_R splitting which is large. Then, \tilde{l}_L has some mass greater than that of $\tilde{\chi}_2^0$, otherwise the charge asymmetry would be washed out or positive. This is likely a typical mSUGRA point.

In summary, the benchmark points of the NG hypothesis from different regions in the (M_{H_u}, M_{H_d}) plane can be readily identified in early 14 TeV running at the LHC, and are easily distinguished from typical mSUGRA points.

5 Conclusions and outlook

The hierarchy of the Yukawa couplings in the standard model remains an open question. We have presented a class of models wherein the first and second generation fermions are SUSY partners of Nambu-Goldstone bosons which parameterize a non-compact Kähler manifold, such that the first and second generation Yukawa couplings are forbidden by the low-energy theorem. Then we gave an (incomplete) example to show that such a model can be constructed.

Next, we found that many different model points in this scenario can give the correct dark matter abundance while easily evading phenomenological bounds, and examined the spectra of benchmark points in different regions of the allowed parameter space. Finally, we argued that these points can be distinguished from conventional mSUGRA points at the LHC, and demonstrated this assuming only 7 fb^{-1} of integrated luminosity at 14 TeV, with $m_{\tilde{g}} \sim 700 \text{ GeV}$.

Nonetheless, improvements can be made. First, explicit models should be constructed, and the consequences of their gravitino and novino fields investigated. Also, the running of the soft masses between the SUSY-breaking and GUT scales should be verified to be small. Second, a more expansive simulation (including backgrounds) should be done with higher integrated luminosity to improve the quality of the endpoint fits and increase the significance of the charge asymmetries. Third, observability at LHC should be verified across the entire (M_{H_u}, M_{H_d}) plane, not only for specific benchmark points.

Finally, we close with two notes on non-LHC phenomenology. First, concerning signatures of dark matter, at model points BP 1 and BP 2 the LSP would be very difficult to detect outside of the LHC. The s -wave annihilations of neutralinos to fermions are helicity-suppressed, and because the LSP at BP 1 and BP 2 is mostly bino, annihilations to the standard model weak bosons are also suppressed. Thus, the total annihilation cross-section is only $\mathcal{O}(10^{-30}) \text{ cm}^3 \text{ s}^{-1}$ in the present universe, far beyond the reach of current or planned astrophysical observatories. On the other hand, at BP 3, the large higgsino component gives a large annihilation cross-section $\mathcal{O}(10^{-26}) \text{ cm}^3 \text{ s}^{-1}$ to W^+W^- . Combined with the low mass, the LSP of BP 3 may be able to explain the anomalous rise in the positron fraction observed by PAMELA [37, 38]; however, the bound from antiprotons [39] must also be checked. Moreover, as discussed, the large higgsino component also enhances the direct detection cross-section. The predicted cross-section $2 \times 10^{-8} \text{ pb}$ is near current limits and therefore within the reach of forthcoming experiments. By contrast, for BP 1 and BP 2, the predicted cross-sections are only $1 \times 10^{-10} \text{ pb}$ and $2 \times 10^{-10} \text{ pb}$, respectively.

Second, the flavor rotations in the quarks and leptons generate flavor-changing transitions among the squarks and sleptons. However, the transition parameter δ_{12} [40] between the first and the second generation is suppressed by λ^5 , where λ is the Wolfenstein parameter [41] in the rotation matrices. Taking $\lambda_d \simeq 0.1$ we see the prediction is very close to the present upper bound on δ_{12} . Interestingly, the transition between the strange and bottom quark is suppressed only by λ_d^2 , which may generate some sizable contributions to the $B_s - \bar{B}_s$ mixing matrix.

In conclusion, we have shown that the NG hypothesis may explain the smallness of the masses of the first and second generation standard model fermions, and that this hypothesis can be tested at the LHC.

Acknowledgments

SKM and MS are supported by World Premier International Research Center Initiative (WPI Initiative), MEXT, Japan. TTY would like to thank T. Kugo for useful discussions.

A Model point data

In this section we give miscellaneous data on the model points:

- Complete listing of masses of new particles (for all model points)
- Plots of invariant mass distributions, with edge fits
- Expected and fit endpoints (as well as secondary endpoints)
- All mass solutions
- Notable branching ratios

Note: All mass units are in GeV.

A.1 Complete listing of masses of new particles

Particle	BP 1	BP 2	BP 3	CP
\tilde{d}_L, \tilde{s}_L	660.4	643.6	639.2	660.2
\tilde{u}_L, \tilde{c}_L	655.5	638.6	634.2	655.3
\tilde{b}_1	1026	1041	998	601.8
\tilde{t}_1	801.6	847.7	742.5	467.8
\tilde{l}_L	158.2	193.7	194.0	222.1
$\tilde{\nu}_{lL}$	136.6	176.5	177.0	207.4
$\tilde{\tau}_1$	1005	1000	999.9	132.6
$\tilde{\nu}_{\tau L}$	1006	1013	1012	206.1
\tilde{d}_R, \tilde{s}_R	641.7	620.4	616.5	634.9
\tilde{u}_R, \tilde{c}_R	619.5	616.8	613.5	635.6
\tilde{b}_2	1159	1159	1156	629.2
\tilde{t}_2	1045	1063	1014	665.8
\tilde{l}_R	205.3	138.3	135.3	144.5
$\tilde{\tau}_2$	1016	1020	1016	225.2
\tilde{g}	730.9	729.3	731.0	721.7
$\tilde{\chi}_1^0$	120.3	120.2	106.3	118.8
$\tilde{\chi}_2^0$	231.7	234.5	166.9	222.0
$\tilde{\chi}_1^\pm$	232.1	234.9	160.4	222.2
$\tilde{\chi}_3^0$	597.8	737.4	203.8	434.5
$\tilde{\chi}_4^0$	606.7	743.6	286.4	451.7
$\tilde{\chi}_2^\pm$	607.2	744.3	282.0	450.7
h^0	115.0	115.3	114.6	116.0
H^0	1293	1071	1176	476.1
A^0	1284	1063	1168	472.8
H^\pm	1295	1073	1179	482.5

Table 6: Listing of masses for model benchmark points and mSUGRA comparison point.

A.2 Benchmark point 1 (BP 1)

A.2.1 True masses

$$m_{\tilde{\chi}_1^0} = 120.3, \quad m_{\tilde{t}} = 158.2, \quad m_{\tilde{\chi}_2^0} = 231.7, \quad m_{\tilde{q}} = 660.4$$

A.2.2 Endpoint values

	m_{ll}^{max}	m_{jll}^{max}	$m_{jl(lo)}^{max}$	$m_{jl(hi)}^{max}$
Expected	109.9	528.5	336.8	451.8
Fit	109.7 ± 0.4	533.3 ± 3.0	341.2 ± 6.0	457.1 ± 2.4

A.2.3 Mass solutions

Region [35]	$m_{\tilde{t}} - m_{\tilde{\chi}_1^0}$	$m_{\tilde{\chi}_2^0} - m_{\tilde{t}}$	$m_{\tilde{q}} - m_{\tilde{\chi}_2^0}$	$m_{\tilde{q}}$
Expected	37.9	73.5	429	660
(1,1)	73.0 ± 1.7	43.1 ± 1.0	459 ± 11	876 ± 62
(1,2)	Imaginary			
(1,3)	37.7 ± 1.1	73.3 ± 1.9	433 ± 7	655 ± 35
(4,1)	Imaginary			
(4,2)	33.3 ± 3.5	76.5 ± 3.0	423 ± 3.2	551 ± 5
(4,3)	37.2 ± 1.3	73.5 ± 2.0	423 ± 3.0	621 ± 15

Correct solution is in bold.

A.2.4 Notable branching ratios

Parent	Daughters	Branching ratio
\tilde{u}_L	$u_L \tilde{\chi}_2^0$	0.33
	$d_L \tilde{\chi}_1^\pm$	0.66
\tilde{u}_R	$u_R \tilde{\chi}_1^0$	1.0
	$u_R \tilde{\chi}_2^0$	1.1×10^{-3}
$\tilde{\chi}_2^0$	$l_L^\pm \tilde{l}_L^\mp$	0.42
	$l_R^\pm \tilde{l}_R^\mp$	5.8×10^{-5}
	$\nu_L \tilde{\nu}_L$	0.58

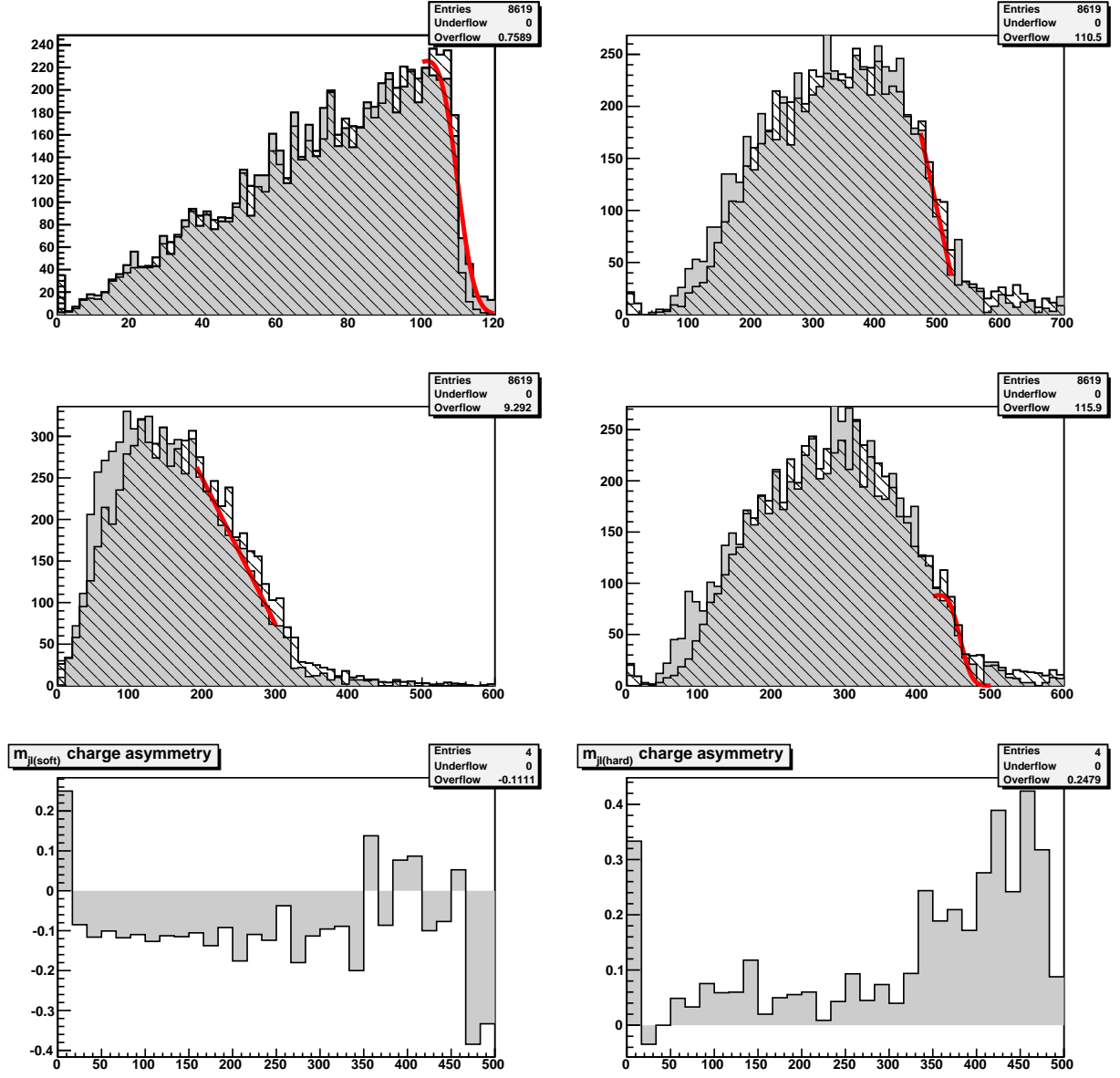


Figure 9: BP 1 invariant mass distributions and endpoint fits. Upper left, m_{ll} ; upper right, m_{jl} ; middle left, $m_{jl(lo)}$; middle right, $m_{jl(hi)}$. Cross-hatched region is parton-level, and solid region is jet-level. Lower left, $m_{jl+(soft)} - m_{jl-(soft)}$; lower right, $m_{jl+(hard)} - m_{jl-(hard)}$.

A.3 Benchmark point 2 (BP 2)

A.3.1 True masses

$$m_{\tilde{\chi}_1^0} = 120.1, \quad m_{\tilde{l}} = 193.7, \quad m_{\tilde{\chi}_2^0} = 234.5, \quad m_{\tilde{q}} = 643.5$$

A.3.2 Endpoint values

	m_{ll}^{max}	m_{jll}^{max}	$m_{jl(lo)}^{max}$	$m_{jl(hi)}^{max}$
Expected	103.7	514.6	337.8	470.0
Fit	103.7 ± 0.3	516.7 ± 1.2	338.0 ± 1.2	468.5 ± 1.9

A fit to the $m_{jl(hi)}$ endpoint with a vertical edge gives $m_{jl(hi)}^{max} = 469.1 \pm 4.8$.

For calculating charge asymmetry, $m_{jl(near)} = 349.5 \pm 2.8$

A.3.3 Mass solutions

Region [35]	$m_{\tilde{l}} - m_{\tilde{\chi}_1^0}$	$m_{\tilde{\chi}_2^0} - m_{\tilde{l}}$	$m_{\tilde{q}} - m_{\tilde{\chi}_2^0}$	$m_{\tilde{q}}$
Expected	73.5	40.8	409	643
(1,1)	72.9 ± 0.7	40.8 ± 0.3	414 ± 3	660 ± 10
(1,2)	Imaginary			
(1,3)	30.0 ± 0.7	75.0 ± 0.8	412 ± 1.4	563 ± 4.6
(4,1)	Imaginary			
(4,2)	23.7 ± 1.2	80.0 ± 1.2	413 ± 1	528 ± 2
(4,3)	30.0 ± 0.7	74.8 ± 0.8	412 ± 1	562 ± 4

Correct solution is in bold.

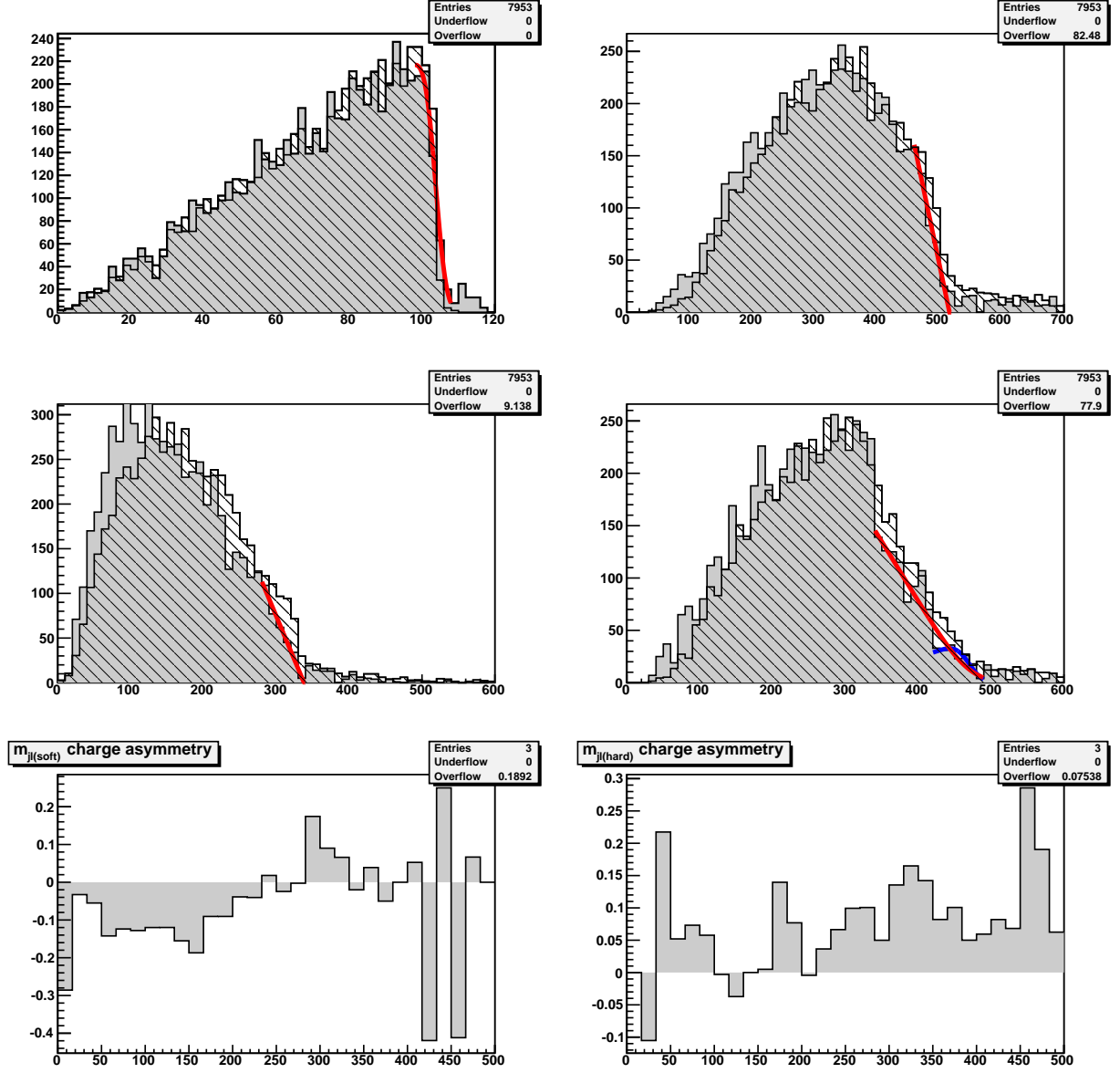


Figure 10: BP 2 invariant mass distributions and endpoint fits. Upper left, m_{ll} ; upper right, m_{jl} ; middle left, $m_{jl(lo)}$; middle right, $m_{jl(hi)}$. For $m_{jl(hi)}$, the red curve is the fit with a ramp function, and the blue curve is the fit with a vertical edge. Cross-hatched region is parton-level, and solid region is jet-level. Lower left, $m_{jl+(soft)} - m_{jl-(soft)}$; lower right, $m_{jl+(hard)} - m_{jl-(hard)}$.

A.3.4 Notable branching ratios

Parent	Daughters	Branching ratio
\tilde{u}_L	$u_L \tilde{\chi}_2^0$	0.33
	$d_L \tilde{\chi}_1^\pm$	0.66
\tilde{u}_R	$u_R \tilde{\chi}_1^0$	1.0
	$u_R \tilde{\chi}_2^0$	5.0×10^{-4}
$\tilde{\chi}_2^0$	$l_L^\pm \tilde{l}_L^\mp$	0.36
	$l_R^\pm \tilde{l}_R^\mp$	5.7×10^{-4}
	$\nu_L \tilde{\nu}_L$	0.64

A.4 Benchmark point 3 (BP 3)

A.4.1 True masses

$$m_{\tilde{\chi}_1^0} = 106.4, \quad m_{\tilde{l}} = 135.3, \quad m_{\tilde{\chi}_2^0} = 166.9, \quad m_{\tilde{q}} = 639.2$$

A.4.2 Endpoint values

	m_{ll}^{max}	m_{jll}^{max}	$m_{jl(lo)}^{max}$	$m_{jl(hi)}^{max}$
Expected	60.4	475.6	324.4	381.4
Fit	60.4 ± 0.1	473.2 ± 4.5	323.3 ± 0.9	370.2 ± 4.4

Secondary edge	m_{ll}^{max}
$\tilde{\chi}_2^\pm \rightarrow \tilde{\nu}_L l^\pm \rightarrow \tilde{\chi}_1^\pm ll$	93.0
$\tilde{\chi}_4^0 \rightarrow \tilde{l}_L l \rightarrow \tilde{\chi}_2^0 ll$	107.4
$\tilde{\chi}_4^0 \rightarrow \tilde{l}_L l \rightarrow \tilde{\chi}_1^0 ll$	176.4

A.4.3 Mass solutions

Region [35]	$m_{\tilde{l}} - m_{\tilde{\chi}_1^0}$	$m_{\tilde{\chi}_2^0} - m_{\tilde{l}}$	$m_{\tilde{q}} - m_{\tilde{\chi}_2^0}$	$m_{\tilde{q}}$
Expected	28.9	31.6	472	639
(1,1)	33.8 ± 0.4	27.3 ± 0.3	580 ± 48	988 ± 170
(1,2)	29.1 ± 1.0	31.4 ± 0.9	491 ± 12	693 ± 31
(1,3)	28.7 ± 1.0	32.1 ± 0.6	437 ± 24	558 ± 50
(4,1)	Imaginary			
(4,2)	38.1 ± 2.2	30.1 ± 0.6	404 ± 6	480 ± 7
(4,3)	30.6 ± 1.0	31.5 ± 0.6	411 ± 5	506 ± 10

Correct solution is in bold.

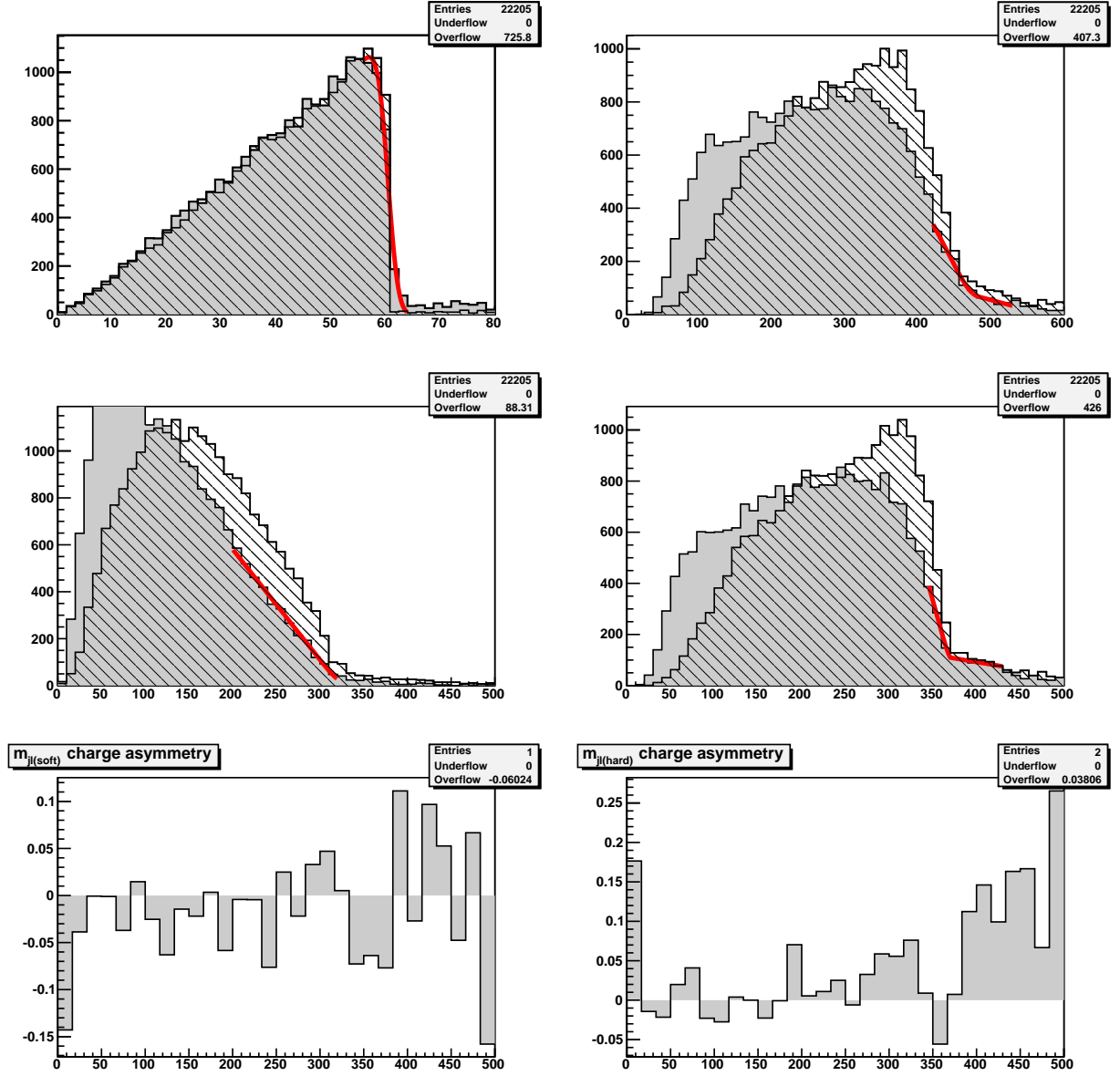


Figure 11: BP 3 invariant mass distributions and endpoint fits. Upper left, m_{ll} ; upper right, m_{jl} ; middle left, $m_{jl(lo)}$; middle right, $m_{jl(hi)}$. Cross-hatched region is parton-level, and solid region is jet-level. Lower left, $m_{jl+}(soft) - m_{jl-}(soft)$; lower right, $m_{jl+}(hard) - m_{jl-}(hard)$.

A.4.4 Notable branching ratios

Parent	Daughters	Branching ratio
\tilde{g}	$q\tilde{q}_L$	0.40
	$q\tilde{q}_R$	0.59
\tilde{u}_L	$u_L\tilde{\chi}_2^0$	0.17
	$u_L\tilde{\chi}_4^0$	0.16
	$d_L\tilde{\chi}_1^\pm$	0.37
	$d_L\tilde{\chi}_2^\pm$	0.30
\tilde{d}_L	$d_L\tilde{\chi}_2^0$	0.095
	$d_L\tilde{\chi}_4^0$	0.19
	$u_L\tilde{\chi}_1^\pm$	0.20
	$u_L\tilde{\chi}_2^\pm$	0.45
\tilde{u}_R	$u_R\tilde{\chi}_1^0$	0.76
	$u_R\tilde{\chi}_2^0$	0.22
$\tilde{\chi}_2^0$	$l_R^\pm\tilde{l}_R^\mp$	1.0
$\tilde{\chi}_4^0$	$l_L^\pm\tilde{l}_L^\mp$	0.21
	$l_R^\pm\tilde{l}_R^\mp$	0.02
	$\nu_L\tilde{\nu}_L$	0.4
$\tilde{\chi}_1^\pm$	$l_L^\pm\nu_L\tilde{\chi}_1^0$	0.36
$\tilde{\chi}_2^\pm$	$l_L^\pm\tilde{\nu}_L$	0.33

A.5 Comparison point (CP)

A.5.1 True masses

$$m_{\tilde{\chi}_1^0} = 118.8, \quad m_{\tilde{l}} = 144.5, \quad m_{\tilde{\chi}_2^0} = 222.0, \quad m_{\tilde{q}} = 666$$

A.5.2 Endpoint values

	m_{ll}^{max}	m_{jll}^{max}	$m_{jl(lo)}^{max}$	$m_{jl(hi)}^{max}$
Expected	95.9	530.3	310.4	476.6
Fit	95.3 ± 0.4	547.6 ± 6.2	309.0 ± 2.7	479.6 ± 15.5

A.5.3 Mass solutions

Region [35]	$m_{\tilde{l}} - m_{\tilde{\chi}_1^0}$	$m_{\tilde{\chi}_2^0} - m_{\tilde{l}}$	$m_{\tilde{q}} - m_{\tilde{\chi}_2^0}$	$m_{\tilde{q}}$
Expected	25.7	77.5	444	666
(1,1)	75.2 ± 3.8	31.6 ± 0.7	526 ± 67	1080 ± 400
(1,2)	Imaginary			
(1,3)	27.6 ± 3.3	76.0 ± 4.5	497 ± 51	848 ± 236
(4,1)	Imaginary			
(4,2)	14.9 ± 3.8	89.0 ± 7.9	444 ± 7	574 ± 10
(4,3)	24.9 ± 2.5	78.3 ± 45.3	444 ± 6	664 ± 30

Correct solution is in bold.

A.5.4 Notable branching ratios

Parent	Daughters	Branching ratio
\tilde{u}_L	$u_L \tilde{\chi}_2^0$	0.32
	$d_L \tilde{\chi}_1^\pm$	0.65
\tilde{u}_R	$u_R \tilde{\chi}_1^0$	0.99
	$u_R \tilde{\chi}_2^0$	4.7×10^{-3}
$\tilde{\chi}_2^0$	$l_R^\pm \tilde{l}_R^\mp$	0.052
	$\tau^\pm \tilde{\tau}_1^\mp$	0.44
	$\nu_L \tilde{\nu}_L$	0.50

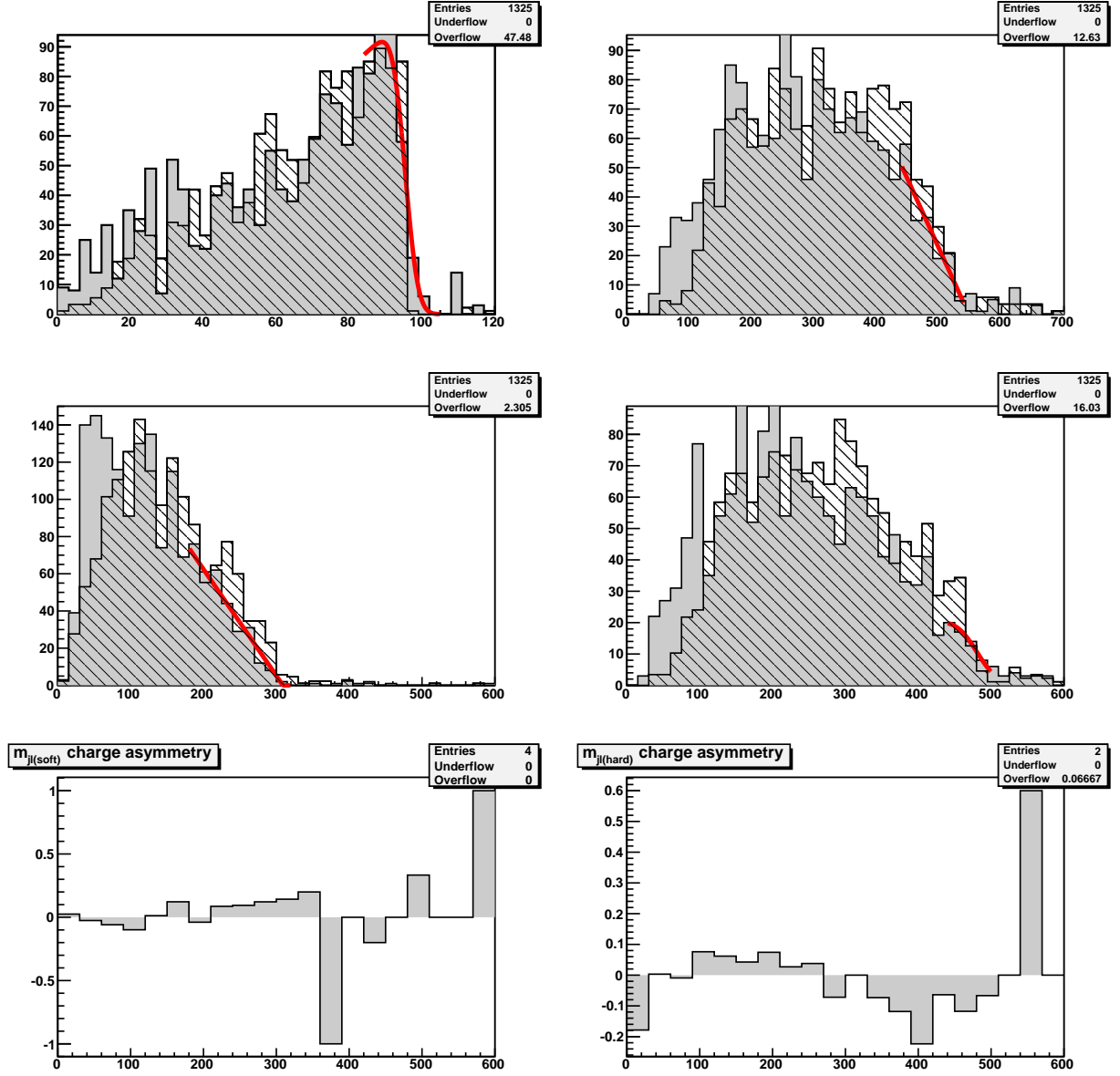


Figure 12: Comparison point invariant mass distributions and endpoint fits. Upper left, m_{ll} ; upper right, m_{jll} ; middle left, $m_{jl(lo)}$; middle right, $m_{jl(hi)}$. Cross-hatched region is parton-level, and solid region is jet-level. Lower left, $m_{jl+(soft)} - m_{jl-(soft)}$; lower right, $m_{jl+(hard)} - m_{jl-(hard)}$.

References

- [1] W. Buchmüller, S. T. Love, R. D. Peccei and T. Yanagida, Phys. Lett. B **115**, 233 (1982).
- [2] W. Buchmüller, R. D. Peccei and T. Yanagida, Nucl. Phys. B **227**, 503 (1983).
- [3] S. L. Adler, Phys. Rev. **137**, B1022 (1965).
- [4] J. Bagger and E. Witten, Phys. Lett. B **118**, 103 (1982).
- [5] T. Kugo, I. Ojima and T. Yanagida, Phys. Lett. B **135**, 402 (1984).
- [6] M. Bando, T. Kuramoto, T. Maskawa and S. Uehara, Prog. Theor. Phys. **72**, 313 (1984).
- [7] T. Kugo and T. T. Yanagida, arXiv:1003.5985 [hep-th]. For another recent discussion of coupling rigid SUSY to supergravity, see Z. Komargodski and N. Seiberg, arXiv:1002.2228 [hep-th].
- [8] J. L. Evans, D. E. Morrissey and J. D. Wells, Phys. Rev. D **75**, 055017 (2007) [arXiv:hep-ph/0611185].
- [9] J. Ellis, A. B. Lahanas, D. V. Nanopoulos and K. Tamvakis, Phys. Lett. B **134**, 429 (1984); J. Ellis, C. Kounnas and D. V. Nanopoulos, Nucl. Phys. B **247**, 373 (1984).
- [10] T. Kugo, S. Uehara and T. Yanagida, Phys. Lett. B **147**, 321 (1984).
- [11] T. Goto and T. Yanagida, Prog. Theor. Phys. **83**, 1076 (1990).
- [12] G. 't Hooft, *Naturalness, chiral symmetry, and spontaneous chiral symmetry breaking*. NATO Adv. Study Inst. Ser. B Phys. **59**, 135 (1980).
- [13] S. Weinberg, Phys. Rev. Lett. **48**, 1303 (1982).
- [14] J. Ellis, D. V. Nanopoulos and S. Sarkar, Nucl. Phys. B **259**, 275 (1985); M. H. Reno and D. Seckel, Phys. Rev. D **37**, 3441 (1988); S. Dimopoulos, R. Esmailzadeh, L. J. Hall and G. D. Starkman, Nucl. Phys. B **311**, 699 (1989); M. Kawasaki, K. Kohri and T. Moroi, Phys. Rev. D **71**, 083502 (2005).
- [15] A. H. Chamseddine, R. Arnowitt and P. Nath, Phys. Rev. Lett. **49**, 970 (1982).
- [16] B. C. Allanach, Comput. Phys. Commun. **143**, 305 (2002), [arXiv:hep-ph/0104145].

- [17] P. Gondolo, J. Edsjo, P. Ullio, L. Bergstrom, M. Schelke and E. A. Baltz, JCAP **0407**, 008 (2004) [arXiv:astro-ph/0406204]; L. Bergström and P. Gondolo, Astropart. Phys. **5**, 263 (1996) [arXiv:hep-ph/9510252]; P. Gondolo and G. Gelmini, Nucl. Phys. B **360**, 145 (1991); J. Edsjö and P. Gondolo, Phys. Rev. D **56**, 1879 (1997) [arXiv:hep-ph/9704361].
- [18] B. Allanach *et al.*, Comput. Phys. Commun. **180**, 8 (2009) [arXiv:0801.0045 [hep-ph]];
- [19] S. Heinemeyer, W. Hollik and G. Weiglein, Comput. Phys. Commun. **124**, 76 (2000) [arXiv:hep-ph/9812320]; S. Heinemeyer, W. Hollik and G. Weiglein, Eur. Phys. J. C **9**, 343 (1999) [arXiv:hep-ph/9812472]; G. Degrandi, S. Heinemeyer, W. Hollik, P. Slavich and G. Weiglein, Eur. Phys. J. C **28**, 133 (2003) [arXiv:hep-ph/0212020]; M. Frank, T. Hahn, S. Heinemeyer, W. Hollik, H. Rzehak and G. Weiglein, JHEP **0702**, 047 (2007) [arXiv:hep-ph/0611326].
- [20] P. Bechtle, O. Brein, S. Heinemeyer, G. Weiglein and K. E. Williams, Comput. Phys. Commun. **181**, 138 (2010) [arXiv:0811.4169 [hep-ph]].
- [21] E. Komatsu *et al.*, arXiv:1001.4538 [astro-ph.CO].
- [22] J. Kopp, T. Schwetz and J. Zupan, JCAP **1002**, 014 (2010) [arXiv:0912.4264 [hep-ph]].
- [23] M. Drees, Y. G. Kim, M. M. Nojiri, D. Toya, K. Hasuko and T. Kobayashi, Phys. Rev. D **63**, 035008 (2001) [arXiv:hep-ph/0007202]; J. Hisano, M. M. Nojiri and W. Sreethawong, JHEP **0906**, 044 (2009) [arXiv:0812.4496 [hep-ph]].
- [24] J. Hisano, K. Nakayama and M. Yamanaka, Phys. Lett. B **684**, 246 (2010) [arXiv:0912.4701 [hep-ph]].
- [25] J. Ellis and K. A. Olive, arXiv:1001.3651 [astro-ph.CO].
- [26] H. Baer, A. Belyaev, T. Krupovnickas and A. Mustafayev, JHEP **0406**, 044 (2004) [arXiv:hep-ph/0403214].
- [27] S. P. Martin, arXiv:hep-ph/9709356.
- [28] P. Richardson, JHEP **0111**, 029 (2001) [arXiv:hep-ph/0110108]; A. J. Barr, Phys. Lett. B **596**, 205 (2004) [arXiv:hep-ph/0405052]; Phys. Rev. D **70**, 075016 (2004) T. Goto, K. Kawagoe and M. M. Nojiri, [Erratum-ibid. D **71**, 059902 (2005)] [arXiv:hep-ph/0406317].

- [29] ATLAS Collaboration, “ATLAS detector and physics performance. Technical design report. Vol. 2,” ATLAS-TDR-15.
- [30] F. E. Paige, S. D. Protopopescu, H. Baer and X. Tata, arXiv:hep-ph/0312045.
- [31] G. Corcella *et al.*, arXiv:hep-ph/0210213.
- [32] E. Richter-Was, arXiv:hep-ph/0207355.
- [33] O. S. . Bruning, *et al.* (ed.), “LHC design report. Vol. I: The LHC main ring,” CERN-2004-003-V-1.
- [34] I. Hinchliffe, F. E. Paige, M. D. Shapiro, J. Soderqvist and W. Yao, Phys. Rev. D **55**, 5520 (1997) [arXiv:hep-ph/9610544]; H. Bachacou, I. Hinchliffe and F. E. Paige, Phys. Rev. D **62**, 015009 (2000) [arXiv:hep-ph/9907518].
- [35] B. K. Gjelsten, D. J. . Miller and P. Osland, JHEP **0412**, 003 (2004)[arXiv:hep-ph/0410303].
- [36] F. James and M. Roos, Comput. Phys. Commun. **10**, 343 (1975). R. Brun and F. Rademakers, Nucl. Instrum. Meth. A **389**, 81 (1997).
- [37] O. Adriani *et al.* [PAMELA Collaboration], Nature **458**, 607 (2009) [arXiv:0810.4995 [astro-ph]].
- [38] M. Cirelli, M. Kadastik, M. Raidal and A. Strumia, Nucl. Phys. B **813**, 1 (2009) [arXiv:0809.2409 [hep-ph]].
- [39] O. Adriani *et al.*, Phys. Rev. Lett. **102**, 051101 (2009) [arXiv:0810.4994 [astro-ph]].
- [40] E. Gabrielli, A. Masiero and L. Silvestrini, Phys. Lett. B **374**, 80 (1996) [arXiv:hep-ph/9509379].
- [41] L. Wolfenstein, Phys. Rev. Lett. **51**, 1945 (1983).